Research Article

Danagul Aubakirova, Elfira Sagymbekova*, Yernat Kozhakhmetov, Piotr Kowalewski, Yerkhat Dauletkhanov, Dias Yerbolat and Azamat Urkunbay

Structural and functional enhancement of Ni–Ti–Cu shape memory alloys via combined powder metallurgy techniques

https://doi.org/10.1515/eng-2025-0140
received July 29, 2025; accepted September 24, 2025

Abstract: This research aims to optimizing the synthesis of Ni–Ti–Cu alloys with shape memory effect (SME) through a combination of mechanosynthesis and spark plasma sintering (SPS). It has been established that the rotation speed (650/750 rpm) and the duration of mechanosynthesis (1–8 h) critically affect the phase composition and morphology of the powders. The speed of the formation of the intermetallic phase NiTi is limited at 650 rpm, whereas it intensifies defect accumulation and amorphization at 750 rpm. X-ray phase analysis and scanning electron microscopy confirmed that the optimal mechanosynthesis regime (8 h, 750 rpm) ensures: synthesis of target phases B2-NiTi and B19′-NiTi; minimal crystallite size (~109 Å); high chemical homogeneity (~46 at% Ni, ~42 at% Ti, ~10 at% Cu). Subsequent SPS at 850–900°C and 49.2 MPa allowed for the production of dense samples. Sintering at 900°C after mechanosynthesis at 750 rpm ensured the predominance of the stable B2 austenitic phase, high microstructural homogeneity, and minimal porosity, which is critical for the reversibility of martensitic transformations. EDS analysis confirmed the chemical homogeneity (~46 at% Ni, ~42 at% Ti, ~10 at% Cu) and the uniform distribution of elements. The results demonstrate the effectiveness of combining mechanosynthesis at an increased rotation speed and reduced duration with SPS for the formation of microstructures optimized for the requirements of shape memory alloy (SMA) materials.

Keywords: Ni–Ti–Cu shape memory alloys, mechanosynthesis, spark plasma sintering, phase transformations, microstructure

1 Introduction

Shape memory alloys (SMAs) represent a class of functional alloys capable of restoring their original shape after plastic deformation due to changes in temperature or under the influence of an external field. This behavior is associated with reversible martensitic phase transformations that occur at the atomic level in the material's crystalline structure [1–4]. The most studied and commercially sought-after are nickel–titanium (NiTi) alloys, which combine high deformability (up to 8% without residual deformation), good corrosion resistance, low elastic modulus, and biocompatibility [5–7]. These characteristics have ensured the widespread use of NiTi alloys in industries such as aerospace, microelectronics, and robotics, as well as in medicine, particularly in the production of cardiovascular stents, orthodontic arches, and surgical instruments [8–14].

The functional properties of NiTi alloys are directly dependent on the mechanism and parameters of the martensitic phase transformation. Upon cooling, the high-temperature austenitic phase with a cubic crystal lattice (B2) transforms into a low-temperature martensitic phase – monoclinic (B19′) or orthorhombic (B19), depending on the alloying additions and processing conditions [3,13,15–18].

*** Corresponding author: Elfira Sagymbekova,** Center of Excellence "VERITAS," D. Serikbayev East Kazakhstan Technical University, Ust-Kamenogorsk, Kazakhstan, e-mail: esagymbekova@edu.ektu.kz
Danagul Aubakirova: Center of Excellence "VERITAS," D. Serikbayev East Kazakhstan Technical University, Ust-Kamenogorsk, Kazakhstan, e-mail: daubakirova@edu.ektu.kz
Yernat Kozhakhmetov: Center of Excellence "VERITAS," D. Serikbayev East Kazakhstan Technical University, Ust-Kamenogorsk, Kazakhstan, e-mail: ykozhakhmetov@edu.ektu.kz
Piotr Kowalewski: Faculty of Mechanical Engineering, Wroclaw University of Science and Technology, Wroclaw, Poland, e-mail: piotr.kowalewski@pwr.edu.pl
Yerkhat Dauletkhanov: Center of Excellence "VERITAS," D. Serikbayev East Kazakhstan Technical University, Ust-Kamenogorsk, Kazakhstan, e-mail: edauletkhanov@edu.ektu.kz
Dias Yerbolat: Center of Excellence "VERITAS," D. Serikbayev East Kazakhstan Technical University, Ust-Kamenogorsk, Kazakhstan, e-mail: dyerbolat@edu.ektu.kz
Azamat Urkunbay: Center of Excellence "VERITAS," D. Serikbayev East Kazakhstan Technical University, Ust-Kamenogorsk, Kazakhstan, e-mail: aurkunbay@edu.ektu.kz

The process is accompanied by the release of latent heat and occurs without diffusion, ensuring high reversibility of the transformation. Upon heating, the reverse transition to the austenitic phase occurs, resulting in the restoration of the original shape of the sample, fixed in the high-temperature state.

One of the ways to enhance the stability and controllability of the shape memory effect (SME) is by alloying the alloys with third elements. Among the numerous additives studied, the most attention is given to copper, which is introduced into the composition in amounts up to 15 at%. The presence of copper in the NiTi system significantly affects phase transformations: as the copper content increases, the crystallography of the martensitic phase changes (B19′ → B19), the thermal hysteresis decreases, and the stability of the SME under cyclic loading increases [3,18–20]. Moreover, NiTiCu alloys demonstrate improved shape-changing characteristics and lower sensitivity to deviations in chemical composition compared to binary NiTi alloys, making them particularly attractive for use under variable thermomechanical loads.

One of the key stages in obtaining functional materials with the SME is the compaction of mechanically activated powders. To achieve the reversible martensitic transformation underlying the SME, it is critically important not only to precisely reproduce the chemical composition but also to ensure a controlled microstructure while maintaining the desired phase nature. Among modern densification technologies, the spark plasma sintering (SPS) method deserves special attention, as it ensures the intensification of mass transfer and phase transformation processes due to the synergistic effect of pulsed electric current, pressure, and temperature.

Unlike traditional sintering methods (vacuum, isostatic, hot pressing), SPS ensures sintering at lower temperatures and in shorter timeframes, which is especially important for SMAs that are sensitive to overheating and grain growth. As shown in [21], SPS allows for the preservation of the nanostructured state of alloys and the stabilization of the B2 phase – a high-temperature cubic crystalline phase, the stability, and proportion of which directly affect the expression of the SME. However, the presence of only the B2 phase is insufficient: during cooling, the realization of a martensitic transformation with the formation of the B19′ phase – a low-temperature monoclinic phase that ensures reversible deformation is necessary. Therefore, the optimal combination of B2 and B19′ phases depending on the operating temperature is a key structural condition for the manifestation of the SME.

This is critically important when Ni–Ti–Cu alloys are processed, where the addition of copper affects both the kinetics of phase transformations and the morphology of the resulting samples. Copper contributes to lowering the temperature of martensitic transformation, stabilizing the B2 phase, and improving the conditions for the formation of the dispersed B19′ phase during cooling, which together promote a more reliable realization of functional properties.

Comparative analysis with alternative approaches [3,22–25] confirms that the combination of mechanosynthesis and SPS allows achieving a highly dispersed and homogeneous structure with minimal porosity and optimal phase composition. Unlike materials obtained solely by mechanical alloying, which often exhibit residual amorphous components or unstable intermediate phases, the application of SPS ensures the formation of a stable matrix with a predominance of the B2 phase and dispersed martensitic B19′ inclusions that form after cooling. Such structural features contribute to the improvement of functional characteristics – an increase in the magnitude of reversible deformation, a decrease in residual deformation, and an enhancement in the stability of thermomechanical loading cycles.

In addition to high density and uniformity, SPS provides an additional advantage – the ability to form target phases at temperatures below the overheating temperatures, which is particularly important for SMA prone to phase instability. NiTi alloys densified by the SPS method demonstrate improved shape memory characteristics due to stabilization of phase composition and prevention of the formation of undesirable phases that alter the reversibility of transformations [26]. In the case of the Ni–Ti–Cu ternary system, the addition of copper contributes to both the reduction of the martensitic transformation temperature and the suppression of oxide inclusion formation, which further enhances the reliability and reproducibility of SMA properties.

Thus, SPS is not only an effective method for powder compaction but also a critically important stage in the technology of synthesizing SMAs. Its application allows the realization of: stabilization of the B2 phase and control of the formation of the B19′ phase during cooling; the formation of a nanostructured matrix necessary for the reproducible SME; increased cyclic stability and reduced residual deformation; and preservation of chemical and structural homogeneity, critically important for the thermomechanical functionality of SMAs.

The results obtained in this study confirm the high efficiency of the combination of mechanosynthesis and SPS for forming a microstructure that ensures the manifestation and the stability of the SME in Ni–Ti–Cu system alloys.

Table 1: Detailed parameters for obtaining a three-component SMA

Mill rotation speed, rpm	Materials (balls/container)	Ball-to-powder ratio	Process duration, min	Atmosphere/Chemical agents
Mixing/mechanosynthesis				
650/750	Stainless steel, 5 mm balls, 45 mL cup	10:1	60/180/300/480	Argon/Stearic acid

Pressure, MPa	Heating rate, °C/min	Holding time, min	Max. temperature, °C	Atmosphere
SPS				
49.2	100	10	850/900	Vacuum

2 Materials and methods

The research objects were samples of the 45Ni–45Ti–10Cu SMA system (at%). The alloys were formed by combining mechanosynthesis and SPS from a three-component powder composition of the Ni–Ti–Cu system (the parameters and scheme are shown in Table 1 and Figure 1). The following powders were used as the starting materials for producing SMAs: nickel powder (main impurities: Si ≤ 0.003; Fe ≤ 0.001; Zr ≤ 0.002; Cu ≤ 0.001; C ≤ 0.002); titanium powder (main impurities: Fe ≤ 0.002; Cr ≤ 0.003; Ni ≤ 0.002; Cu ≤ 0.003; Ta ≤ 0.002); copper powder (main impurities: Al ≤ 0.002; Fe ≤ 0.001; Cr ≤ 0.001; Ni ≤ 0.001; Si ≤ 0.002) with a particle size <50 μm and a purity of 99%, obtained from Hebei Suoyi New Material Technology, Hebei Province, China.

Eight samples were compared under various mechanosynthesis modes. To carry out the mechanosynthesis process, a planetary micro mill (*Pulverisette 7 Premium Line*, Fritsch GmbH, Idar-Oberstein, Germany) was used. Based on the analysis of the phase composition and morphology of the powders obtained after mechanosynthesis, optimal conditions were selected for subsequent densification using the SPS method. The specified parameters were chosen based on the literature data [1–3,19– 23,26] and initial experiments as the most suitable for the effective densification of powder blanks while preserving and stabilizing the previously formed B2 and B19′ phases responsible for the SME, as well as minimizing undesirable phase transformations.

To assess the influence of temperature parameters on the densification process, shrinkage kinetics were analyzed for powder compacts prepared under optimal mechanosynthesis

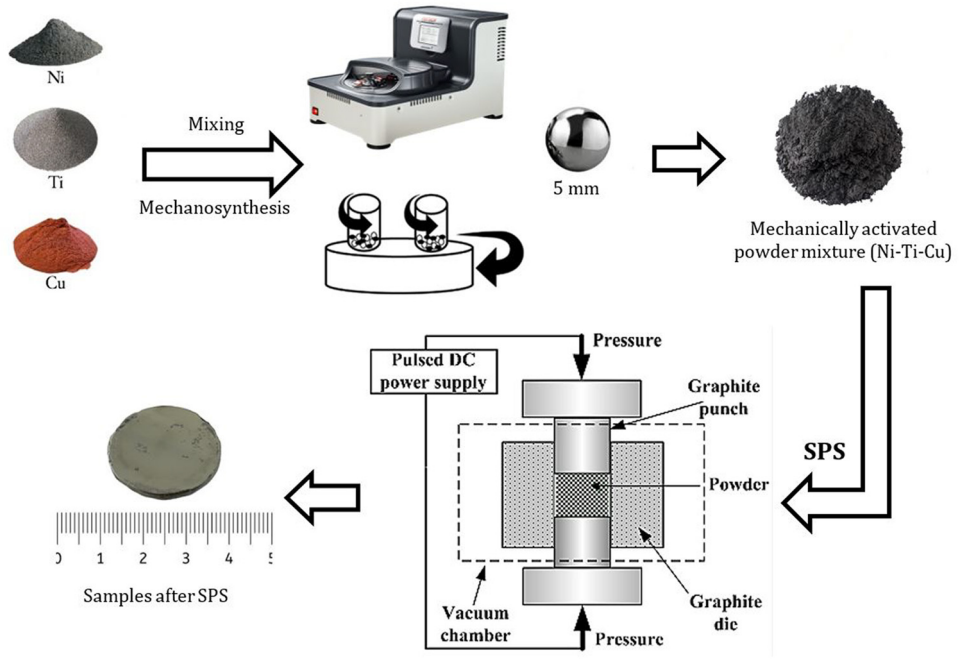

Figure 1: Scheme for obtaining SMAs based on the Ni–Ti–Cu system.

conditions and sintered at various temperatures. Both samples exhibit a characteristic three-stage shrinkage curve (Figure 2): I – initial densification during heating (up to ~650 °C), II – intensive shrinkage in the isothermal regime (~650–850/900 °C), and III – stabilization upon reaching the final density. For the sample sintered at 850 °C (curve (1)), the intensive shrinkage stage (II) begins approximately at the first minute of the isothermal holding. The maximum shrinkage rate reaches ~8.9 × 10^{-3} mm/s, with a total linear deformation of ~1.6 mm. At 900 °C (curve (2)), intensive shrinkage starts slightly earlier, almost immediately after reaching the isothermal plateau. In this case, the shrinkage rate increases to ~1.27 × 10^{-2} mm/s, and the final shrinkage reaches ~1.9 mm. The more pronounced densification at 900 °C compared to 850 °C may be attributed to the intensification of diffusion processes and the reduction in material flow resistance, which together promote more efficient powder consolidation during sintering.

The samples obtained after sintering were prepared for examination on a Struers grinding-polishing machine using water cooling. During the surface preparation, the samples were sequentially polished on silicon carbide grinding paper with grit sizes: P400–600–800–1200, and then subjected to polishing on polishing cloths with the addition of diamond suspensions, with particle sizes of 3 and 1 μm. To reveal the microstructure, the samples were subjected to chemical etching, using a solution of a mixture of concentrated nitric acid HNO_3 (65–68 wt%) and hydrochloric acid HCl (32–35 wt%), taken in a volume ratio of 1:3 (mass ratio, when recalculated to pure substances is about 1:2). The samples were analyzed to assess the phase composition, microstructure, and morphological changes that occurred during the densification process.

The analysis of the crystalline characteristics and phases of the alloy samples was conducted using an X-ray diffractometer *X'Pert PRO* (Malvern Panalytical Empyrean, Netherlands) with a copper anode. The measurement was conducted in the angle range of 2θ = 20–100 °, with a tube voltage of 45 kV and a current of 40 mA. The scan step was 0.02 °, and the accumulation time at each step was 1.5 s. Diffraction patterns were processed using the *HighScore* program for phase identification and analysis. The evolution of morphology was studied using a scanning electron microscope (SEM) (*Phenom ProX*, Thermo Fisher Scientific, USA), and the particle size distribution was analyzed with a laser diffraction analyzer (*Analysette 22 NeXT Nano*, Fritsch, Germany).

3 Results and discussion

Figures 3 and 4 show the intermetallic phases B2-NiTi and B19′-NiTi. All reference diffraction patterns were obtained from the ICSD and COD databases. The corresponding card numbers are listed below:

- B2-NiTi – ICSD: 98-016-0482;
- B19′-NiTi – ICSD: 98-016-1458;
- Ni – COD: 96-210-0650;
- Ti – COD: 96-900-8518;
- Cu – COD: 96-901-3015.

The X-ray diffractogram (XRD) presented in Figure 3 demonstrates the phase evolution of a multicomponent

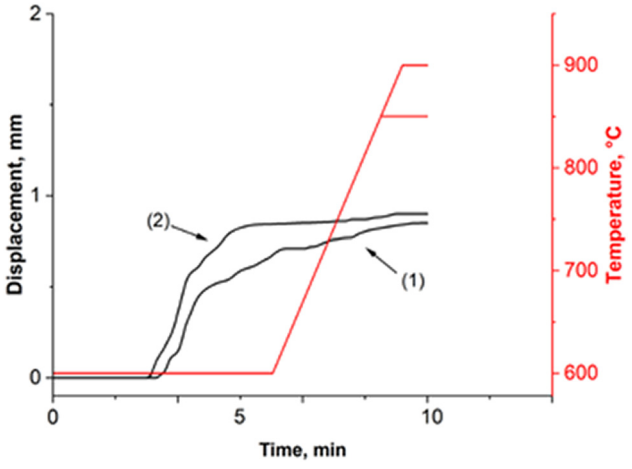

Figure 2: Shrinkage curves of Ni–Ti–Cu powder compacts sintered by SPS at 850 and 900 °C.

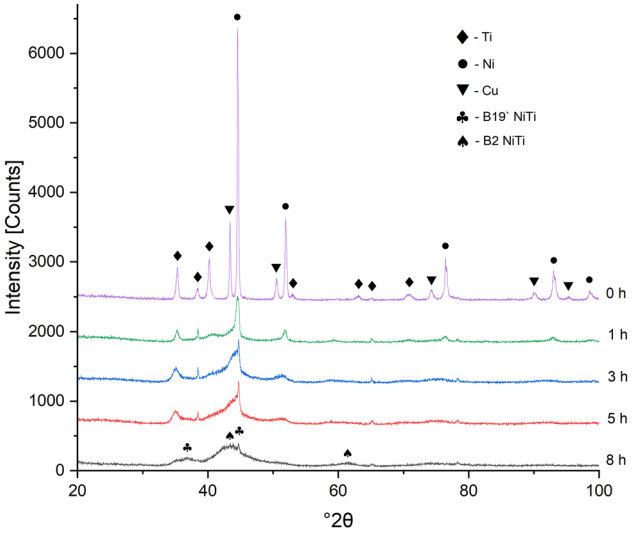

Figure 3: X-ray diffractogram of the Ni–Ti–Cu powder mixture after mechanosynthesis at 650 rpm for different durations.

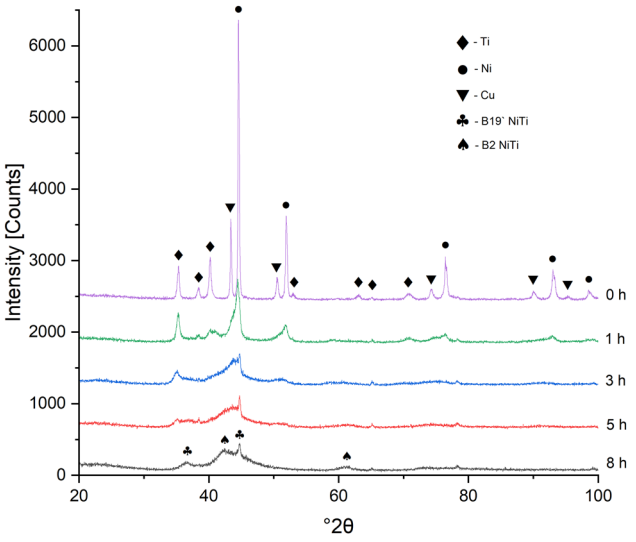

Figure 4: X-ray diffractogram of the Ni–Ti–Cu powder mixture after mechanosynthesis at 750 rpm for different durations.

metallic system subjected to mechanosynthesis at a rotation speed of 650 rpm over various time intervals (from 0 to 8 h). Intense and narrow diffraction peaks corresponding to the phases Ti, Ni, and Cu are clearly observed in the initial mixture (0 h) at the initial stage, indicating a high degree of crystallinity of the initial mixture and the absence of any significant phase transformations. As the processing time increases, a gradual decrease in intensity and broadening of the main reflections is observed, indicating the accumulation of structural defects, a reduction in crystallite size, and an increase in internal stress within the materials. However, even after 8 h of mechanosynthesis, pronounced peaks of Ni and Ti remain, and the formation of the new NiTi phase remains weakly expressed, indicating the limited reactivity of the system at this energy level.

The obtained data indicate the inadequacy of the kinetic conditions created at 650 rpm for intensifying solid-phase chemical interactions between the components of the mixture. Thus, the processes of mechanical dispersion and particle deformation at a relatively low rotation speed, rather than their chemical transformation, exert the main influence. The results emphasize that the mechanical energy introduced into the system at 650 rpm is marginal and insufficient for the effective synthesis of the NiTi phase, which is manifested in the preservation of the initial phase composition and high degree of crystallinity throughout the entire processing. This confirms the need to increase the impact energy (e.g., by increasing the rotation speed) to initiate target reactions and form new phases with a more pronounced chemical nature.

The dynamics of changes in the phase composition and degree of crystallinity of the material, observed in the X-ray diffraction patterns of the samples shown in Figure 4, underwent intensive mechanosynthesis at a rotation speed of 750 rpm over a period of 1–8 h, indicating deep structural-phase transformations occurring under the influence of high-energy plastic deformation. The initial mixture (0 h) also demonstrates well-resolved, narrow, and high-intensity diffraction peaks corresponding to the phases of pure metals Ti, Ni, and Cu, indicating a coarse crystalline structure with a high degree of long-range order.

A progressive broadening and decrease in peak intensity is observed with an increase in time to 1–3 h, reflecting a reduction in crystallite size to the nanometer range (estimated using the Scherrer formula) and the accumulation of microstrains due to dislocation strengthening, which is consistent with the mechanism of deformation-diffusional crystal lattice breakdown. The appearance and the growth of NiTi intensity indicate the development of solid-phase chemical reactions induced by mechanosynthesis, involving active defect centers formed during grain fragmentation.

A qualitative shift in the material's structure is observed at the 5 h stage of mechanosynthesis: the peaks become broad and poorly defined, and the suppression of the main reflections of the initial phases is recorded, indicating the dominance of amorphization and cooperative diffusion processes at the grain boundaries. The sharp diffraction maxima completely disappear by the 8th hour, and the structure acquires an amorphous or quasi-amorphous character with minor fluctuations in the background (halo-like profile), indicating the achievement of a state of complete loss of long-range order.

These results highlight the key role of the duration and intensity of activation in controlling the phase evolution of the material.

It is noteworthy that after just 1 h of milling, the peaks corresponding to elemental copper completely disappear in both modes. This is likely due to the dissolution of copper in the NiTi-based solid solution or its amorphization as a result of intense plastic deformation and defect accumulation during high-energy milling. This observation indicates the high reactivity and mobility of copper under mechanochemical conditions.

As already noted, with the increase in milling time, a systematic broadening and decrease in the intensity of diffraction peaks is observed, indicating the formation of a nanocrystalline structure and the development of internal microstrains. These changes are more pronounced in samples processed at 750 rpm compared to 650 rpm,

indicating more intense structure milling and increased defect accumulation at higher collision energies. Thus, a higher rotation speed contributes to accelerated grain destruction and intensification of plastic deformation.

Crystallite size and lattice strain were calculated using the Scherrer method with the built-in calculator in HighScore Plus software (Malvern Panalytical). For each diffraction peak, the position (2θ) and full width at half maximum were determined. Based on these parameters, the software automatically calculated the crystallite size and microstrain using standard Scherrer equations. For each sample, the calculations were performed using all identified diffraction peaks, and then the average values of crystallite size and lattice strain were determined. The most prominent peaks were used for semi-amorphous samples obtained after 8 h of milling. All values have been rounded according to the method's accuracy, and measurement errors are provided accordingly.

The calculated values of crystallite sizes and microstrain confirm the aforementioned observations. The crystallite size decreases from 292.8 Å (0 h) to 108.8 Å (8 h) at 750 rpm, while the microstrain of the crystal lattice increases from 0.28 to 1.79%. Meanwhile, the crystallite size reduces to 144.7 Å, and the microstrain reaches 1.61% after 8 h of milling at 650 rpm (Table 2). These data demonstrate that a higher processing intensity contributes to both deeper structural milling and an increase in internal stresses due to the accumulation of defects and dislocations.

Despite the fact that at speeds of 650 and 750 rpm, structural transformation processes – specifically, the reduction of crystallite sizes and the increase in microstrains – occur with significantly greater intensity, and the formation of intermetallic phases – ordered cubic B2-NiTi (lattice parameter a = 3.0150 Å) and martensitic monoclinic B19′-NiTi – are observed only after 8 h of mechanical alloying in both modes. This indicates that, regardless of the differences in milling kinetics, the transition to the ordered phase is due to the necessity of reaching a critical level of accumulated defects and activating interatomic diffusion processes, which are only realized with sufficient duration and energy of mechanochemical processing.

Table 2: Deformation of the powder mixture lattice depending on milling time

Time (h.)	650 rpm		750 rpm	
	Size (Å)	Strain (%)	Size (Å)	Strain (%)
0	292 ± 29	0.3 ± 0.1	292 ± 29	0.3 ± 0.1
1	269 ± 27	0.4 ± 0.1	232 ± 23	0.9 ± 0.1
3	223 ± 22	1.2 ± 0.1	215 ± 22	1.3 ± 0.1
5	200 ± 20	1.4 ± 0.1	165 ± 17	1.4 ± 0.1
8	145 ± 15	1.6 ± 0.1	109 ± 11	1.8 ± 0.1

The morphology of the Ni–Ti–Cu alloy powder before the start of mechanosynthesis is clearly visible in Figure 5a. The particles are predominantly spherical in shape, with a smooth surface and weakly expressed signs of deformation, which indicates the preservation of the initial powder morphology after the initial mixing stage. There are individual fragments of various shapes, but large rounded particles with sizes of approximately 31 and 46.8 μm predominate. The average particle size in this state significantly exceeds the sizes observed in the subsequent stages, reflecting the absence of intensification of plastic deformation and material disintegration.

As a result of intensive mechanical impact for 1 h (Figure 5b), morphological changes already begin at 650 rpm. The particles lost their sphericity and took on an irregular, angular shape, which is typical for processes of plastic deformation and fracture during high-energy milling. Large aggregates with pronounced granulation are visible, with sizes ranging from 39.6 to 53.8 μm. Despite the fact that the average particle size visually remained comparable to the original, a clear increase is observed in dispersion – both smaller and larger particles appear. This indicates the competition between two processes: grinding and aggregation, which is the characteristic of the intermediate stages of mechanosynthesis, when the impact energy is already sufficient for local plastic deformation, but the steady-state grinding mode has not been reached yet.

There is a sharp decrease in the average grain size to 17.1 μm or less after 3 h (Figure 5c), indicating the intensification of the crushing process. An extensive fraction of fine particles appears, covering the surface of larger agglomerates. The particles become even more dispersed, and slightly larger formations appear after 5 h (Figure 5d), which is likely due to secondary agglomeration from cold welding.

In the SEM image after 8 h (Figure 5e), it can be seen that the average particle size has slightly increased compared to 5 h, which is likely due to the dominance of agglomeration processes over fragmentation. The particles acquire a rounded shape, indicating multiple acts of plastic deformation and cold welding. It is evident that the stage of grinding has stopped and that structural stability has started in comparison to the earlier time points.

SEM images obtained at a processing speed of 750 rpm demonstrate pronounced morphological changes occurring even at early stages (Figure 6). After 1 h of processing, the appearance of cracking and active destruction zones is observed, with the average grain size decreasing to

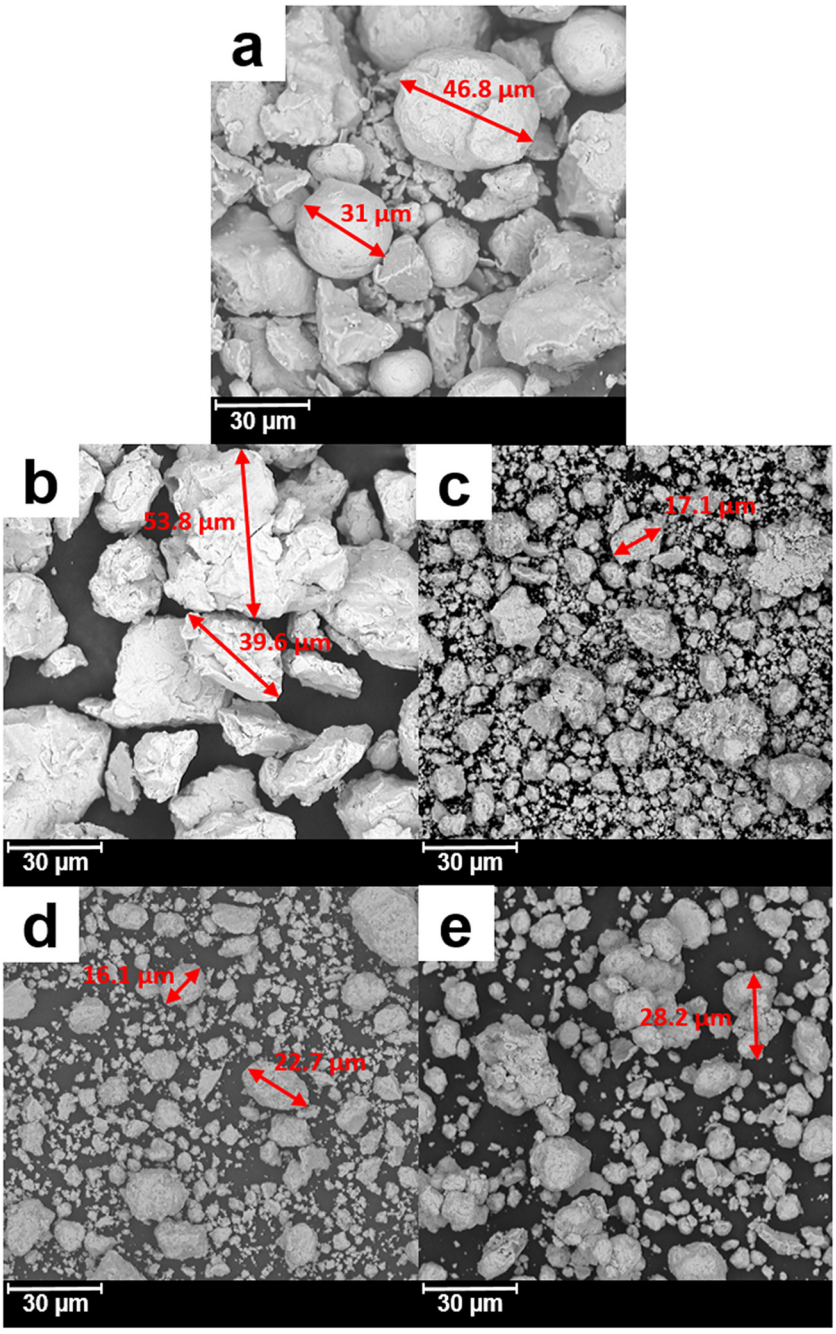

Figure 5: SEM images of the Ni–Ti–Cu powder mixture subjected to mechanosynthesis at 650 rpm for different durations: (a) initial powder mixture; (b) after 1 h; (c) after 3 h; (d) after 5 h; and (e) after 8 h.

25.9 µm, as shown in Figure 6a. By 3 h, the formation of a highly dispersed mass with submicron and nanostructured formations is observed, among which rounded particles with a diameter of less than 1 µm predominate, indicating the presence of nanoscale formation, which is identical for 5 h as well (Figure 6b). These particles exhibit signs of agglomeration, likely due to localized temperature increases during intense collisions.

Morphological stabilization is achieved by 5 h and further by 8 h (Figure 6c and d): conglomerates of submicron and nanostructured particles are present, surrounded by residual inclusions. There is a noticeably more intense reduction in grain sizes here, as well as the formation of structures typical of reactive activated systems in comparison with 650 rpm. The presence of fine-dispersed clusters may indicate the emergence of reactivity in the system,

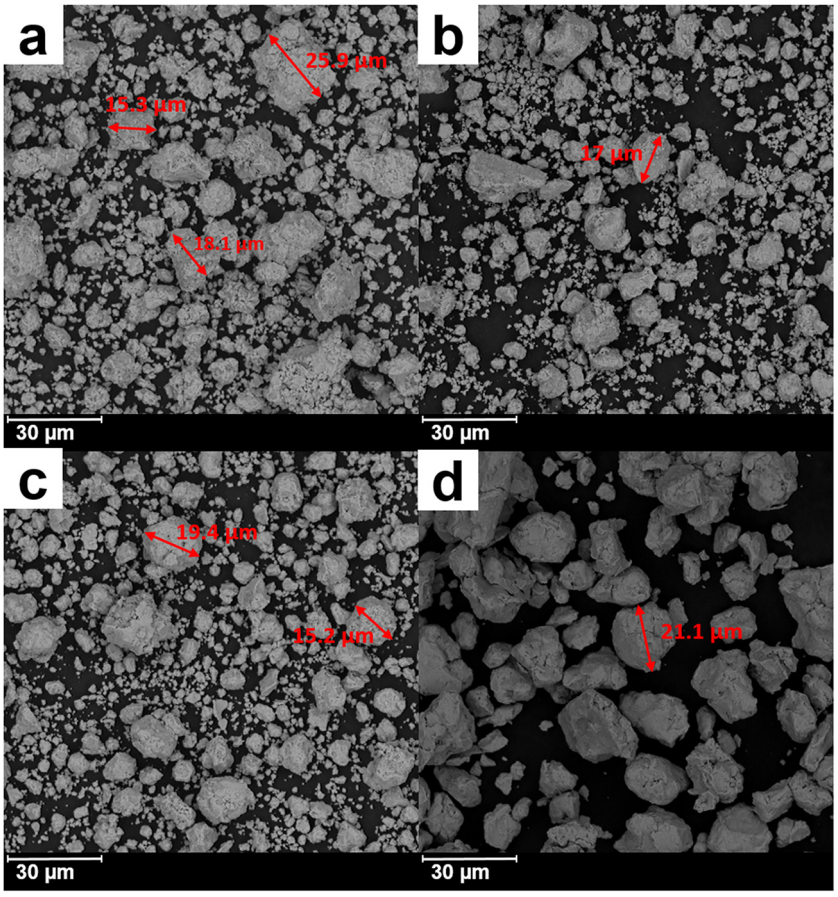

Figure 6: SEM images of the Ni–Ti–Cu powder mixture subjected to mechanosynthesis at 750 rpm for different durations: (a) after 1 h; (b) after 3 h; (c) after 5 h; and (d) after 8 h.

especially after 8 h, when the surface becomes distinctly pronounced and heterogeneous.

Thus, a more pronounced effect of mechanosynthesis is achieved at 750 rpm with an enlarged interfacial interaction zone and minimal grain size. Microstructural changes clearly correlate with X-ray phase analysis and confirm the dominance of dispersion processes over reaction transformation under limited energy conditions at 650 and 750 rpm.

The analysis of SEM images demonstrates a clear dependence of particle morphology on rotation speed and processing duration. Fragmentation occurs more slowly at 650 rpm, and agglomeration begins to dominate by 5–8 h, leading to grain coarsening. At the same time, particle milling occurs significantly faster at 750 rpm, reaching maximum dispersion within 3–5 h, with a stable retention of the fine-dispersed phase. The average grain size at 650 rpm stabilizes at around ~11 µm, and the formation of nanoparticles begins, while it starts to increase after 8 h at 750 rpm.

From the perspective of SMA structure formation, the stage with maximum dispersion is optimal for subsequent sintering, as the reduced grain sizes contribute to accelerated diffusion, the formation of a uniform phase, and the potential improvement of SMA functional properties, such as reversible deformation and phase transition stability. Thus, increasing the rate of mechanochemical processing contributes to the intensification of plastic deformation processes, accelerated particle breakdown, and stabilization of nanostructured morphology, which is crucial for the subsequent phase formation and functional properties of the Ni–Ti–Cu composite.

For the quantitative assessment of the chemical composition and confirmation of the homogeneity of Ni–Ti–Cu powders obtained by the mechanosynthesis method, a point energy-dispersive X-ray spectroscopy (EDS) analysis was performed. The study was conducted on eleven different surface areas of the particles, as shown in Figure 7. The results demonstrate the following ranges of element concentrations:

- Nickel (Ni): 44.7–46.8 at%;
- Titanium (Ti): 40.2–43.7 at%;
- Copper (Cu): 11.1–13.2 at%.

The analysis results confirm a high degree of chemical homogeneity of the powders obtained through mechanosynthesis. Minor deviations, for example, in copper content (Spectrum 6 and Spectrum 10), are likely related to local fluctuations at the early stages of the diffusion interaction of the components. However, the deviations do not exceed 2 at%, which falls within the acceptable technological limits.

EDS spectra show clearly defined peaks of the corresponding elements (Ni, Ti, Cu), with no impurities, confirming the high purity of the system and the effectiveness of the mechanical synthesis parameters used (650–750 rpm, 8 h of processing). The quantitative composition data are consistent with the reference on mechanically alloyed Ni–Ti–Cu system alloys [27,28] and demonstrate the potential of the obtained powders for further densification by SPS to produce shape memory materials.

Additionally, microstructural visualization using SEM and energy-dispersive element mapping were conducted to assess the morphology and spatial distribution of Ni, Ti, and Cu in the powders. In the SEM image (Figure 8a), agglomerates of irregularly shaped particles are clearly visible, formed as a result of processes such as plastic deformation, cold welding, and brittle fracture during high-energy milling.

Mapping of element distribution shows an even distribution of nickel (Figure 8b), titanium (Figure 8c), and copper (Figure 8d) throughout the studied area. This indicates the formation of a homogeneous solid-phase during the mechanosynthesis process, which is critically

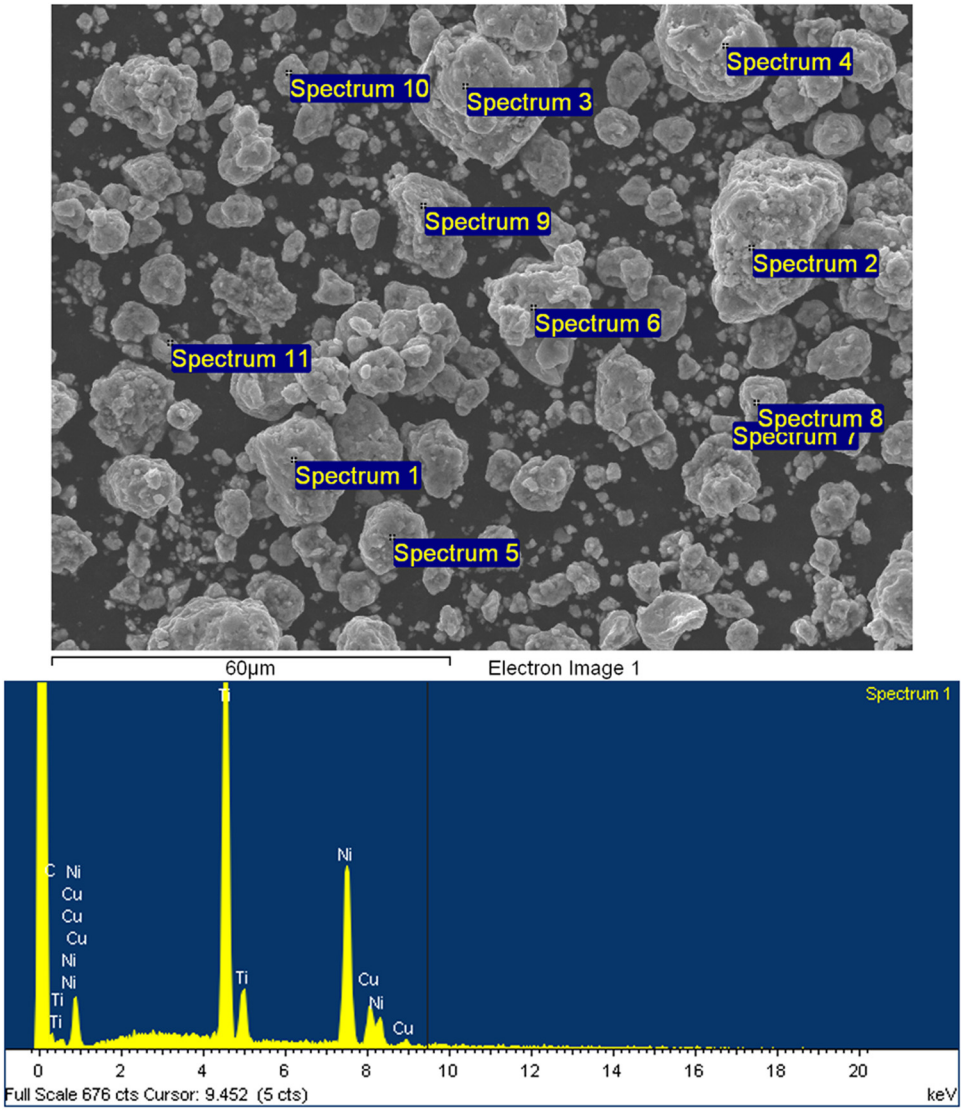

Figure 7: Results of point energy-dispersive X-ray spectroscopy using SEM.

important for SMAs, where the NiTi phase must be as pure and uniform as possible.

The obtained images confirm the initial stage of intermetallic compound formation and are consistent with previously published studies, where mechanical alloying led to effective mixing of components and activation of diffusion processes [29]. The visual and quantitative homogeneity of the composition makes these powders suitable for subsequent densification by the SPS method, which will ensure the production of functional alloys with reproducible thermomechanical properties.

A cross-sectional analysis of the powder mixture of the Ni–Ti–Cu system was conducted for a more detailed study of the microstructure and element distribution within the volume of the material after mechanosynthesis. This allowed us to assess the degree of homogenization within the depth of the particles and identify possible impurities related to sample preparation. Figure 9 presents the results of the cross-sectional analysis of the Ni–Ti–Cu powder mixture obtained by the mechanosynthesis method. The SEM image (Figure 9(a)) demonstrates a high degree of agglomeration and contact between particles, indicating intense interfacial interactions during the mechanosynthesis process. The results of elemental mapping confirm the uniform distribution of the main elements – Ni (Figure 9(b)), Ti (Figure 9(c)), and Cu (Figure 9(d)) – throughout the volume of the analyzed area. The absence of signs of pronounced segregation indicates effective homogenization of the mixture and the formation of a multicomponent composition.

The results of the local energy dispersive analysis show that the ratio of the main elements is approximately 46.2 ± 0.5 at% Ni, 42.5 ± 0.4 at% Ti, and 10.1 ± 0.5 at% Cu, which is close to the specified initial composition. In certain points, the presence of small amounts of silicon (Si), chromium (Cr), and iron (Fe) was recorded, which were absent in the initial powder after mechanosynthesis; their total content does not exceed a few atomic percent. The occurrence of these impurities is explained by the specifics of sample preparation: in particular, the use of abrasive grinding paper with oxides and metal inclusions, as well as the conductive thermosetting resin *Struers PolyFast*, which contains fillers based on inorganic and metal components. During the grinding and polishing process, particles from the abrasive and resin could have embedded into the near-surface layer of the sample, causing false signals in the EDS spectrum. Thus, the identified impurities are not related to the mechanosynthesis process but are artifacts of sample preparation.

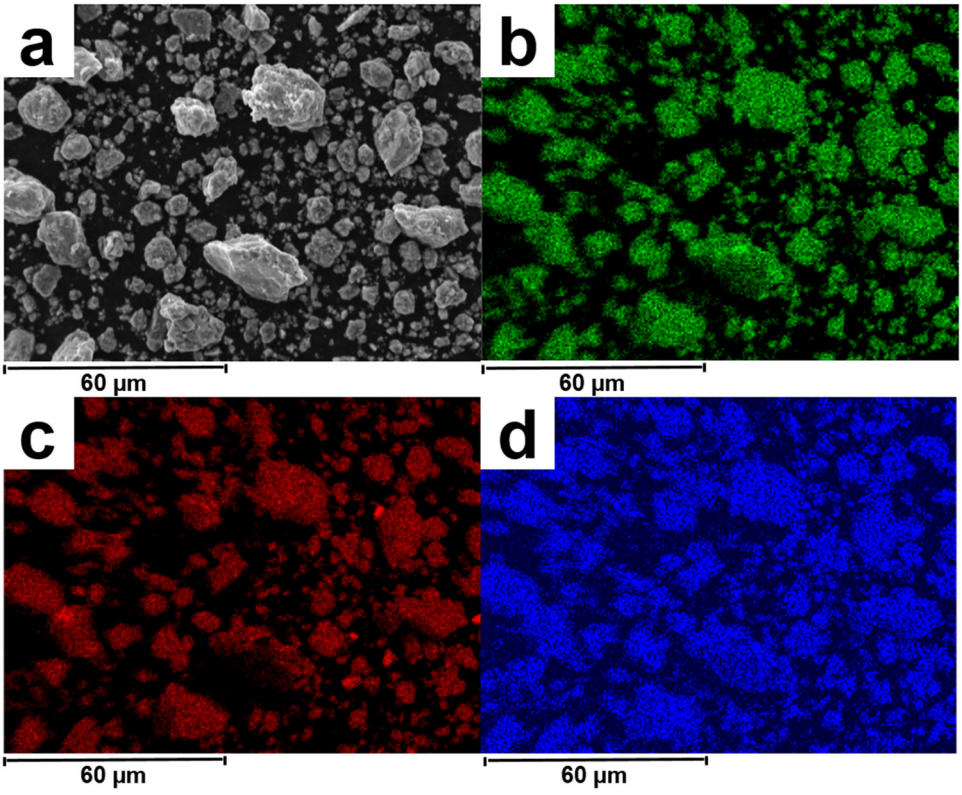

Figure 8: Mapping the microstructure of Ni–Ti–Cu powders after mechanosynthesis.

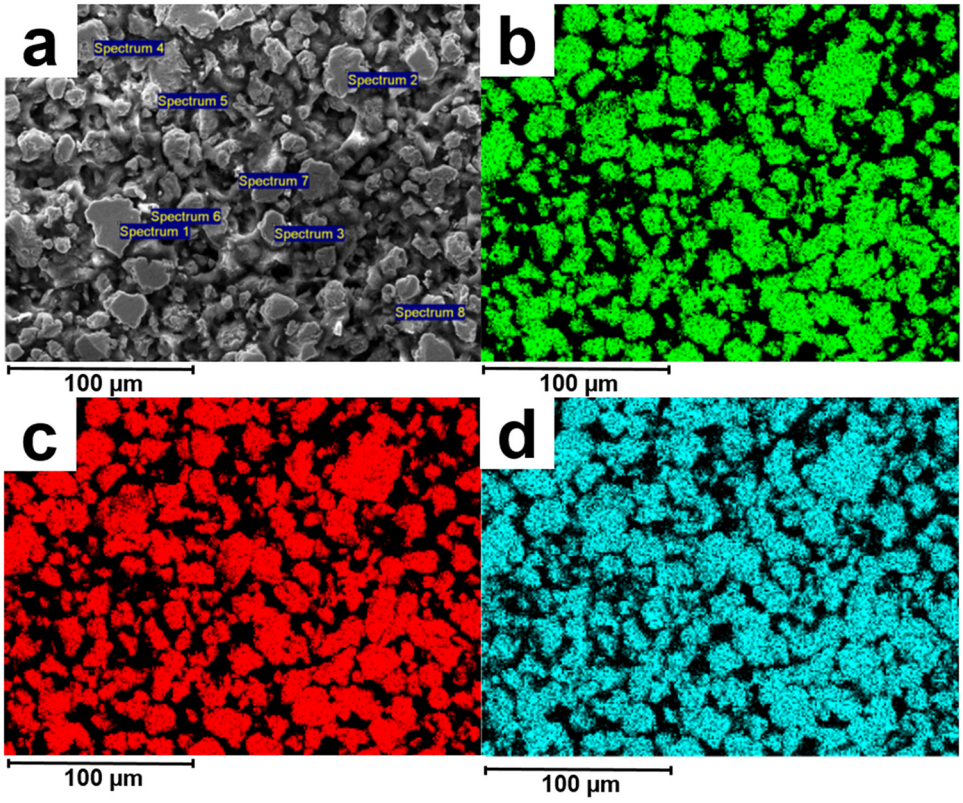

Figure 9: SEM image and elemental mapping of the cross-section of the Ni–Ti–Cu powder mixture after mechanosynthesis.

It should be noted that the behavior of powders during machining is largely determined by the crystalline structure and physicochemical characteristics of the constituent elements. Thus, titanium possesses a hexagonally close-packed lattice with a limited number of slip systems, a high melting point, and pronounced deformation hardening, which contributes to the accumulation of dislocations and the active destruction of its structure in the early stages of machining [27]. In contrast, nickel, which has a face-centered cubic (FCC) structure with a greater number of slip systems and a lower level of deformation hardening, deforms more plastically, which limits the level of defect accumulation in the initial period of milling [30,31].

The addition of copper, which also has an FCC structure, has a dual effect on the milling and activation process. On one hand, copper can act as a soft phase, facilitating lubrication and redistribution of mechanical energy in the system, reducing the likelihood of cold welding [32]. On the other hand, it increases the number of potential diffusion interaction sites with titanium and nickel due to the higher mobility of the ionic lattice, which under prolonged mechanical processing conditions can contribute to the earlier onset of solid-phase reactions [33,34]. In the SEM images, rounded agglomerates and areas with a homogeneous microstructure are observed, indicating the redistribution of material and interphase diffusion between particles. Such morphological features confirm the occurrence of solid-phase reactions during mechanical processing [31,33]. Moreover, the lower melting point of copper compared to Ti and Ni expands the temperature window for the onset of recrystallization processes, which affects the morphological evolution and the formation of nanostructured phases [33,34].

An analysis of the average particle sizes was conducted using an analyzer for a quantitative assessment of morphological changes (Figures 10 and 11). The obtained data demonstrate a clear dependence of particle size on the duration and speed of processing. The initial size was approximately 28.7 μm. After 1 h of processing at a speed of 650 rpm, no significant reduction in size due to agglomeration is observed, whereas by 3–5 h, effective particle grinding occurs. However, an increase in size is again observed by 8 h, attributed to the dominance of cold welding processes due to high activation.

The grinding dynamics are more pronounced at 750 rpm: the particle size becomes smaller than at 650 rpm after just 1 h, and the minimum dispersion is achieved by 3–5 h. There is a tendency towards agglomeration by

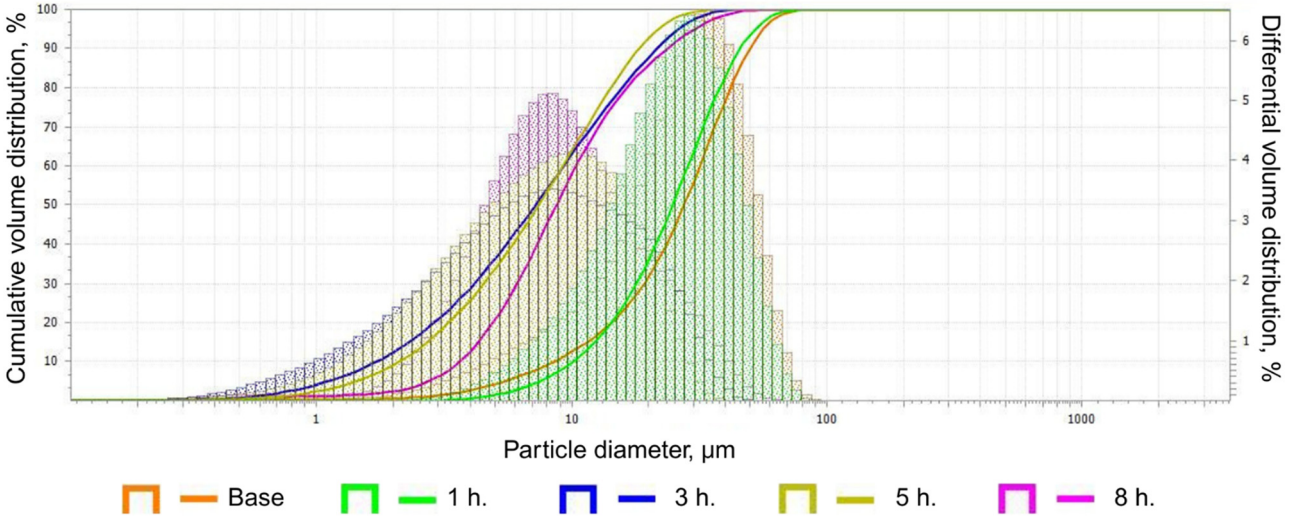

Figure 10: Particle size distribution after mechanosynthesis at 650 rpm.

the 8th hour of mechanosynthesis at 750 rpm; however, the structure remains coarser compared to the 650 rpm mode, where the powder mixture is more finely dispersed.

The results demonstrate that the optimal mechanosynthesis time to achieve the minimum particle size is 3–5 h in both modes (650 and 750 rpm) (Table 3). However, despite the particle growth by 8 h, it is at this processing duration that the target phases B2 and B19′, responsible for shape memory, are formed, as confirmed by X-ray phase analysis. This highlights the need for a compromise between milling parameters and the requirements for the material's phase composition.

Considering the identified connection between morphological changes and mechanosynthesis regimes, the next step was to study the phase composition of the obtained alloys after SPS to assess the stability and nature of the formed phases.

Figure 12 shows the X-ray diffraction patterns of NiTiCu alloys obtained by SPS under different temperature regimes. Three main phases were identified in both samples: the austenitic B2 phase (cubic structure, a = 3.0150 nm; ICSD No. 98-016-0482), the martensitic B19′ phase (monoclinic structure, a = 2.8860 nm, b = 4.1130 nm, c = 4.6310 nm; ICSD No 98-024-0195), and the intermetallic

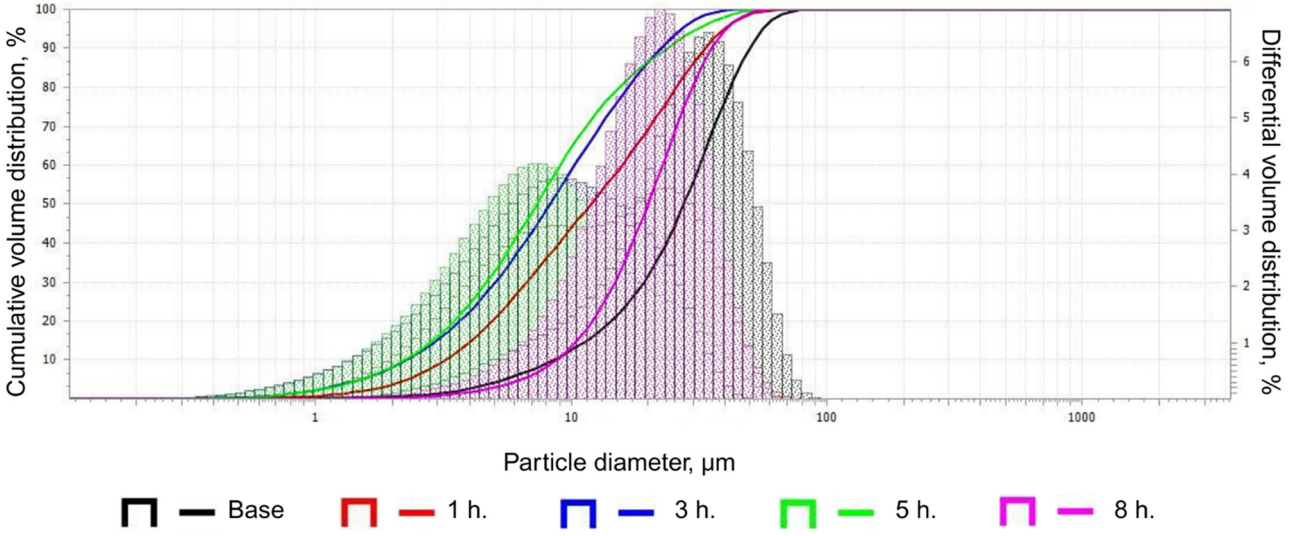

Figure 11: Particle size distribution after mechanosynthesis at 750 rpm.

Table 3: Results of EDS analysis (SEM) of Ni–Ti–Cu powder

Milling time (h)	Average particle size at 650 rpm (μm)	Average particle size at 750 rpm (μm)
0	28.7 ± 0.57	28.7 ± 0.57
1	26.6 ± 0.53	15.6 ± 0.31
3	9.7 ± 0.19	10.5 ± 0.21
5	9.0 ± 0.18	10.4 ± 0.20
8	11.4 ± 0.23	21.2 ± 0.42

Ni_4Ti_3 phase (hexagonal structure, a = 11.6230 nm, c = 5.0969 nm; ICSD No 98-016-6373). The sharp and intense diffraction peaks indicate the formation of a highly ordered crystalline structure, which is attributed to active recrystallization occurring at sintering temperatures exceeding 0.6 T_m (T_m – the melting temperature of the NiTiCu alloy). This process is accompanied by grain growth and a reduction in lattice microstrain [35]. Quantitative phase analysis using the Rietveld method confirms these observations. At the sintering temperature of 850 °C, the phase composition includes 29.7% NiTi B2 (austenite), 42.6% NiTi B19′ (martensite), and 27.7% Ni_4Ti_3. When the sintering temperature is increased to 900 °C, the fraction of the B2 phase increases to 34.4%, the content of B19′ martensite decreases to 40.9%, and the amount of Ni_4Ti_3 phase is reduced to 24.6%. These results quantitatively confirm the trend revealed by the qualitative X-ray phase analysis: increasing the sintering temperature promotes the stabilization of the B2 austenite phase and reduces the amount of secondary Ni_4Ti_3 precipitates, while a noticeable fraction of B19′ martensite is still retained.

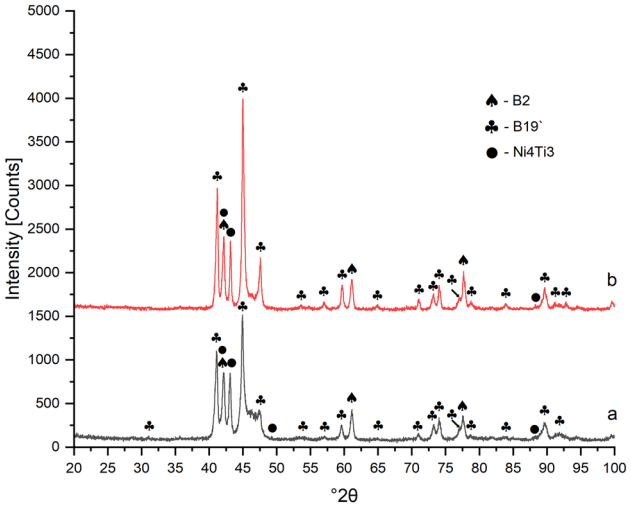

Figure 12: X-ray diffraction patterns of Ni–Ti–Cu alloys after SPS at 850 and 900 °C.

At the sintering temperature of 850 °C (sample a), a relatively high intensity of the martensitic B19′ phase peaks and a noticeable presence of the Ni_4Ti_3 intermetallic phase are observed. This is consistent with SEM/EDS results indicating chemical inhomogeneity due to local segregation of nickel and copper. Specifically, regions enriched with nickel up to 53.79 at% were detected, which promotes the formation of the Ni_4Ti_3 phase. Such phase distribution can be attributed to insufficient homogenization at this temperature, resulting in incomplete stabilization of the B2 phase and its partial transformation into B19′ martensite during cooling.

In contrast, when the sintering temperature is increased to 900 °C (sample b), the diffraction pattern is dominated by intense B2 phase peaks, while the B19′ and Ni_4Ti_3 peaks are significantly suppressed. This reflects a more homogeneous alloy microstructure (Figure 13), as well as a reduced compositional variability in copper (ΔCu = 3.05 at%). This phase behavior is driven by enhanced diffusion processes at the higher temperature, which promote stabilization of the B2 phase and suppress nickel segregation.

The presence of the Ni_4Ti_3 phase in both samples can be attributed to the kinetics of the SPS process, during which local nickel enrichment (e.g., in the region of Spectrum 4) creates favorable conditions for the formation of this phase during rapid heating and subsequent cooling. The reduced intensity of the Ni_4Ti_3 diffraction peaks at 900 °C confirms improved homogenization, which is consistent with the EDS results showing a decrease in chemical anomalies. It should be emphasized that the Ni_4Ti_3 intermetallic phase in the investigated samples is present in the form of finely dispersed precipitates. This is evidenced by the relatively low intensity and noticeable broadening of the Ni_4Ti_3 diffraction peaks in the XRD patterns. Finely dispersed, coherent or semi-coherent Ni_4Ti_3 precipitates in Ni–Ti–Cu alloys play a crucial role in improving the reversibility of the martensitic transformation, reducing hysteresis, and enhancing cyclic stability. These precipitates induce elastic stresses and local Ni-depletion in the matrix, promoting more distinct and reproducible martensite–austenite nucleation [36]. Their homogeneous distribution within grains suppresses dislocation accumulation during repeated thermal and mechanical cycling, thereby extending the durability of shape memory and pseudoelastic behavior [37]. Under high strain rates, Ni_4Ti_3 precipitation also raises the transformation stress and stabilizes the transformation [38]. Consequently, optimally formed Ni_4Ti_3 precipitates may serve as effective regulators of transformation temperatures, suppress irreversible strains, and ensure stable and reproducible shape memory performance.

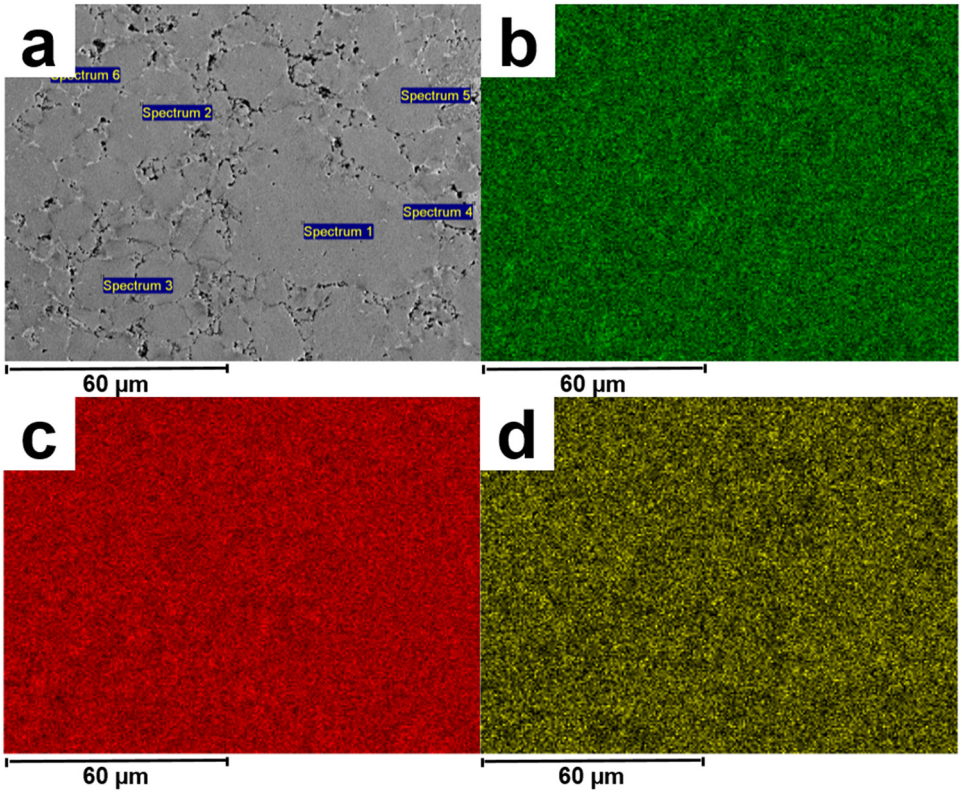

Figure 13: SEM image and elemental mapping of the Ni–Ti–Cu after SPS 850 °C.

The analysis of the relationship between phase composition and synthesis parameters indicates that increasing the heating rate from 650 °C/min to 750 °C/min – when transitioning from 850 °C to 900 °C – promotes more complete diffusion processes despite the holding time remaining constant (10 min). In addition, increasing the mechanosynthesis speed to 750 rpm during the preparation of sample b resulted in finer powder dispersion, enhancing their reactivity during the sintering process.

Thus, increasing the SPS temperature from 850 °C to 900 °C shifts the phase equilibrium toward the austenitic B2 phase, as evidenced by a more than 40% increase in the intensity of its corresponding diffraction peaks. At the same time, the formation of the martensitic B19′ phase and the Ni_4Ti_3 intermetallic is suppressed. However, the residual presence of B19′ even at 900 °C can be explained by a combination of factors, including local stresses in areas with residual porosity and slight deviations from the nominal stoichiometry of 45Ni–45Ti–10Cu (at%) – in particular, the average nickel content was found to be 48.64 at%, exceeding the nominal value.

As a technological recommendation for complete suppression of the B19′ and Ni_4Ti_3 phases, it is proposed to increase the SPS temperature to 920–950 °C and to optimize the mechanosynthesis parameters to eliminate nickel-enriched local zones. A comprehensive analysis of the obtained data suggests that the 900 °C/10 min regime represents an optimal compromise between microstructural homogeneity, phase purity, and the technological feasibility of the process.

The surface morphology and elemental distribution in 45Ni–45Ti–10Cu (at%) alloys after SPS were investigated using SEM and EDS.

Sample 1 (850 °C, 10 min): The SEM image (Figure 13(a)) reveals a developed porous microstructure with pronounced intergranular voids and heterogeneous contrast, indicating both phase and chemical inhomogeneity. EDS analysis (Figure 13(b)–(d)) confirmed the presence of all primary alloying elements, where Figure 13(b) corresponds to Ni, Figure 13(c) to Ti, and Figure 13(d) to Cu. The average elemental composition across six spectra was: Ti – 38.03 ± 3.89 at%, Ni – 48.22 ± 3.49 at%, and Cu – 12.45 ± 1.87 at%. Minor impurities were also recorded: V – 0.09 ± 0.21 at%, Cr – 0.05 ± 0.11 at%, and Fe – 0.80 ± 0.23 at%, while Si was nearly absent (0.04 ± 0.10 at%). Such deviations indicate insufficient diffusion homogenization at this sintering temperature.

According to X-ray diffraction data, this sample shows a relatively high content of the martensitic B19′ phase. This

is consistent with the observed microstructural and chemical inhomogeneity, as well as the presence of localized deformation in porous areas and residual stresses due to incomplete recrystallization. The locally elevated copper content promotes stabilization of the B19′ martensite phase.

Sample 2 (900 °C, 10 min): This sample (Figure 14a) is characterized by a dense, uniform structure with a clearly defined grain morphology and significantly reduced porosity (SEM analysis indicates a 30–40% decrease in porosity compared to Sample 1 after SPS at 850 °C). The increase in sintering temperature enhanced mass transport, enabling more complete diffusion homogenization and recrystallization.

According to the EDS analysis (Figure 14b–d), a markedly improved chemical homogeneity was achieved, where Figure 14b corresponds to Ni, Figure 14c to Ti, and Figure 14d to Cu. The average composition of the main elements was: Ti – 38.32 ± 3.40 at%, Ni – 48.64 ± 3.78 at%, Cu – 11.49 ± 1.07 at%. These values are much closer to the nominal composition of NiTiCu compared to Sample 1 (Ti – 38.03 at%, Ni – 48.22 at%, Cu – 12.45 at%).

The variability in copper content significantly decreased (ΔCu = 2.91 at% versus 6.32 at% in Sample 1). However, the variation in nickel remained relatively high (ΔNi = 11.23 at%), due to a single spectrum (Spectrum 7) with abnormally high Ni content (56.36 at%). Trace amounts of vanadium (up to 0.06 ± 0.15 at%, with a maximum of 0.40 at% in Spectrum 7) were also detected, confirming their localized origin likely from the tooling.

The X-ray diffraction patterns of this sample show sharp, intense peaks corresponding to the B2 (austenite) phase, indicating the formation of a well-ordered crystalline structure. The reduced intensity of the B19′ martensitic phase peaks compared to Sample 1 reflects the dominance of the B2 phase (estimated at >85% versus >60% in Sample 1). This is a direct result of the improved microstructural homogeneity, reduced internal stresses, and effective thermal stabilization of the austenite phase at the elevated sintering temperature.

The density of the samples was measured using the hydrostatic Archimedes method. After SPS at 850 °C, the density was 4260 kg/m^3, whereas at 900 °C, it increased to 4725 kg/m^3. The increase in density indicates a reduction in residual porosity and is consistent with the microstructural analysis (Figure 14), which shows improved grain boundary cohesion and enhanced alloy homogeneity at 900 °C. Thus, the comprehensive analysis clearly

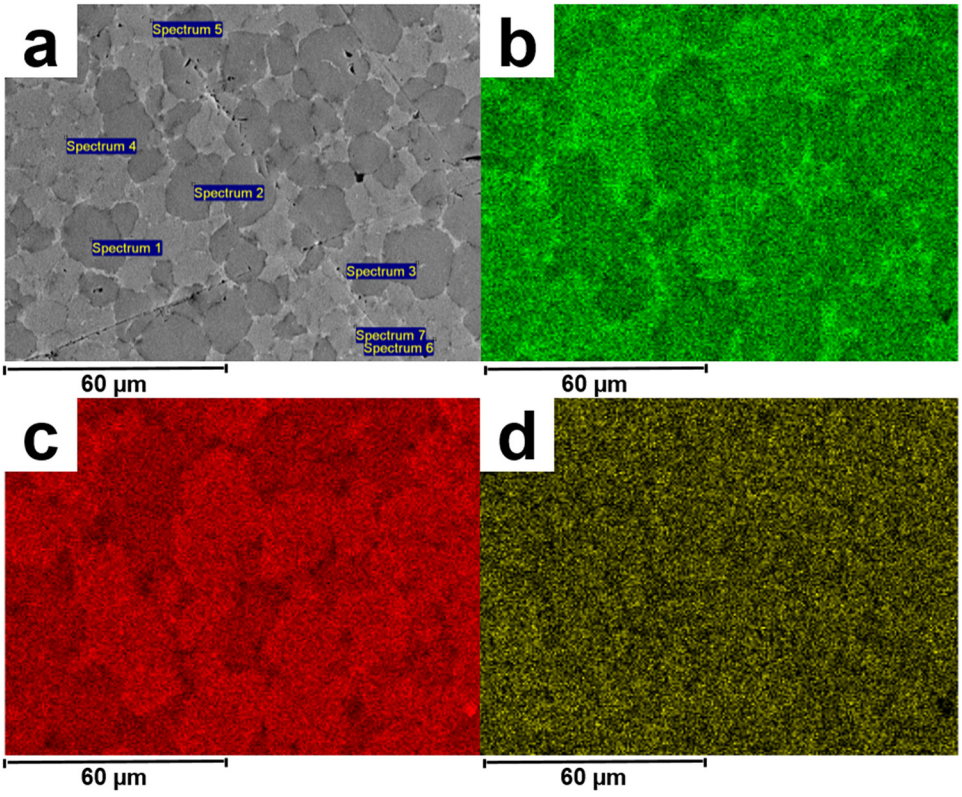

Figure 14: SEM image and elemental mapping of the Ni–Ti–Cu after SPS 900 °C.

demonstrates that increasing the SPS temperature from 850 °C to 900 °C under otherwise identical conditions (holding time of 10 min) leads to: (i) the formation of a dense, low-porosity microstructure with well-defined grain boundaries; (ii) a significant improvement in the chemical homogeneity of the alloy, particularly in copper distribution; (iii) stabilization of the high-temperature austenitic B2 phase; and (iv) suppression of the martensitic B19′ phase formation.

The primary reason for these observed improvements is the activation of diffusion processes and recrystallization at the elevated temperature, which ensures more complete compositional homogenization and the release of internal stresses. To achieve the highest possible homogeneity and full stabilization of the target B2 phase in Ni–Ti–Cu alloys, further investigation of SPS regimes with extended isothermal holding times appears to be a promising direction.

4 Conclusion

This research presents an integrated method for producing intermetallic Ni–Ti–Cu SMAs, based on the sequential application of mechanosynthesis and SPS. It was established that the mechanical alloying stage leads to the formation of the ordered B2–NiTi phase in the powder state, while subsequent SPS induces the formation of the martensitic B19′–NiTi phase, indicating the potential for reversible martensitic transformation in the synthesized materials.

Morphological analysis showed that increasing the rotation speed during mechanical alloying and raising the SPS temperature enhance grain formation, improve interparticle contact, and enable high densification with a homogeneous microstructure. EDS confirmed a uniform distribution of nickel, titanium, and copper throughout the material, which is a critical condition for the stable manifestation of functional properties.

The sample produced at a rotation speed of 750 rpm and an SPS temperature of 900 °C exhibited optimal structural and phase organization, characterized by dominant B2-phase content, high chemical homogeneity, and a dense structure, all of which provide favorable conditions for reversible martensitic transformation.

The obtained results demonstrate the high efficiency of the proposed technological route and its applicability in the development of thermosensitive actuators, sensors, and other functional components based on Ni–Ti–Cu alloys.

Funding information: This research was funded by the Science Committee of the Ministry of Science and Higher Education of the Republic of Kazakhstan (Grant No. AP22682739).

Author contributions: All authors have accepted responsibility for the entire content of this manuscript and consented to its submission to the journal, reviewed all the results, and approved the final version of the manuscript. D.A.: conceptualization, methodology, formal analysis, writing – original draft preparation; E.S.: conceptualization, methodology, formal analysis, writing – original draft preparation; Y.K.: conceptualization, methodology, formal analysis, writing – original draft preparation, supervision; P.K.: conceptualization, formal analysis, writing – original draft preparation; D.Y.: conceptualization, methodology, writing – original draft preparation; A.U.: conceptualization, formal analysis.

Conflict of interest: The authors state no conflict of interest.

Data availability statement: The data are contained within the article.

References

[1] Noor S, Abdulrazzaq M, Amar A. Effect of ball milling on NiTi powder metallurgy alloy. Al-Qadisiyah J Eng Sci. 2022;15:208–11. doi: 10.30772/qjes.v15i3.840.

[2] Cirstea CD, Lucaci M, Valeanu M, Sofronie M, Bujoreanu LG, Lungu MV, et al. Studies about structural and thermal investigations on Ti50Ni30Cu20 alloys obtained by different technological processes. Rom J Phys. 2021;66:601.

[3] Cirstea CD, Povoden-Karadeniz E, Cirstea V, Tolea F, Kozeschnik E. Thermodynamic and kinetic simulations used for the study of the influence of precipitates on thermophysical properties in NiTiCu alloys obtained by spark plasma sintering. Nanomaterials. 2024;14:461. doi: 10.3390/nano14050461.

[4] Cirstea CD, Pintea J, Cirstea V, Popa M, Ilie C, Marin M. Thermal and electrical properties of phase change materials obtained by spark plasma sintering. Rom J Phys. 2025;70:601. doi: 10.59277/RomJPhys.2025.70.601.

[5] Gil FJ, Planell JA. Shape memory alloys for medical applications. Proc Inst Mech Eng H J Eng Med. 1998;212(6):473–88.

[6] Bil C, Massey K, Abdullah EJ. Wing morphing control with shape memory alloy actuators. J Intel Material Syst Struct. 2013;24(7):879–98.

[7] Hartl DJ, Lagoudas DC. Aerospace applications of shape memory alloys. Proc Inst Mech Eng G J Aerospace Eng. 2007;221(4):535–52.

[8] Stoeckel D. Shape memory actuators for automotive applications. Materials Design. 1990;11(6):302–7.

[9] Butera F, Coda A, Vergani G. Shape memory actuators for automotive applications. Nanotec IT Newsletter. Roma: AIRI: Nanotec IT; 2007. p. 12–6.
[10] Kheirikhah MM, Rabiee S, Edalat ME. A review of shape memory alloy actuators in robotics. In: Robot Soccer World Cup. Berlin, Heidelberg: Springer; 2010. p. 206–17.
[11] Stephen D, Sreekumar M, Nagarajan T, Singaperumal M, Zoppi M, Molfino R. Critical review of current trends in shape memory alloy actuators for intelligent robots. Indust Robot Int J. 2007;34(4):285–94.
[12] Petrini L, Migliavacca F. Biomedical applications of shape memory alloys. J Metallurgy. 2011;2011:501483. doi: 10.1155/2011/501483.
[13] Manjaiah M, Narendranath S, Basavarajappa S. Review on non-conventional machining of shape memory alloys. Trans Nonferrous Metals Soc China. 2014;24(1):12–21.
[14] Skakov M, Miniyazov A, Batyrbekov E, Baklanov V, Koyanbayev Y, Gradoboev A, et al. Influence of the carbidized tungsten surface on the processes of interaction with helium plasma. Materials. 2022;15:7821. doi: 10.3390/ma15217821.
[15] Wilson J, Weselowsky M. Shape memory alloys for seismic response modification: A state-of-the-art review. Earthquake Spectra. 2005;21:569–601.
[16] Dong J, Cai C, Okeil A. Overview of potential and existing applications of shape memory alloys in bridges. J Bridge Eng. 2011;16:305–15.
[17] Ponhan K, Tassenberg K, Weston D, Nicholls K, Thornton R. Effect of SiC nanoparticle content and milling time on the microstructural characteristics and properties of Mg-SiC nanocomposites synthesized with powder metallurgy incorporating high-energy ball milling. Ceramics Int. 2020;46(17):26956–69. doi: 10.1016/j.ceramint.2020.07.173.
[18] Auditee MM, Fahmida G, Ehtsham U, Fathima L, Syed AM. Fast sintering of copper-based shape memory alloys for biomedical applications: design, fabrication and characterization. Materials Today. 2024;64:28–37.
[19] Bor A, Jargalsaikhan B, Uranchimeg H, Lee J, Choi H. Particle morphology control of metal powder with various experimental conditions using ball milling. Powder Tech. 2021;394:181–90. doi: 10.1016/j.powtec.2021.08.053.
[20] Joy J, Krishnamoorthy A, Tanna A, Kamathe V, Nagar R, Srinivasan S. Recent developments on the synthesis of nanocomposite materials via ball milling approach for energy storage applications. Appl Sci. 2022;12:9312. doi: 10.3390/app12189312.
[21] Li G, Meng X, Geng C, Wang C, Ren H, Guo X, et al. Microstructure and properties of AlxCr1-xCoFeNi high-entropy alloys prepared by spark plasma sintering. Materials. 2025;18:755. doi: 10.3390/ma18040755.
[22] Velmurugan C, Senthilkumar V, Kesavan J, Ramya K. Effects of sintering temperature on grain growth of NiTiCu shape memory alloy. Materials Today Proc. 2020;39:1570–4. doi: 10.1016/j.matpr.2020.05.704.
[23] Velmurugan C, Senthilkumar V, Biswas K, Yadav S. Densification and microstructural evolution of spark plasma sintered NiTi shape memory alloy. Adv Powder Tech. 2018;29(10):2456–62. doi: 10.1016/j.apt.2018.06.026.
[24] Mukhamedova N, Kozhakhmetov Y, Skakov M, Kurbanbekov S, Mukhamedov N. Microstructural stability of a two-phase (O + B2) alloy of the Ti-25Al-25Nb system (at%) during thermal cycling in a hydrogen atmosphere. AIMS Materials Sci. 2022;9(2):270–82.
[25] Kozhakhmetov YA, Skakov MK, Kurbanbekov SR, Mukhamedov NM, Mukhamedov NY. Powder composition structurization of the Ti-25Al-25Nb (at%) system upon mechanical activation and subsequent spark plasma sintering. Eurasian Chem-Tech J. 2021;23(1):37–44. doi: 10.18321/ectj1032.
[26] Abdul'menova E, Kul'kov SN. Ti-Ni powder structure after mechanical activation and interaction with hydrogen. Russian Phys J. 2019;61:1360–7. doi: 10.1007/s11182-019-01873-y.
[27] Scudino S, Surreddi KB, Sordelet DJ, Eckert J. Formation and thermal stability of nanostructured Ni-Ti alloys prepared by mechanical alloying. Acta Mater. 2012;60:682–91.
[28] Calka A, Wexler D. Mechanical alloying of Ti-Ni intermetallics using controlled milling energies. J Alloys Compounds. 2010;497:132–6.
[29] Estrin Y, Ivanisenko Y, Valiev R. Grain refinement and phase formation in Cu-containing shape memory alloys synthesized by high-energy milling. Mater Sci Eng A. 2015;640:241–8.
[30] Shuai Y, Liu Y, Wang Y, Li X, Zhang J, Sun H, et al. Mechanical alloying of immiscible metallic systems: Process, microstructure, and mechanism. Adv Eng Mater. 2021;23(4):2001098. doi: 10.1002/adem.202001098.
[31] Suryanarayana C. Mechanical alloying: A novel technique to synthesize advanced materials. Research. 2019;2019:4219812. doi: 10.34133/2019/4219812.
[32] Chérif A, Bachaga T, Saurina J, Benali Y, Haddad A, Khatir Z, et al. Morphology and structure effect of Ti additive on the solid-state reaction between Ni and Al powders during mechanical alloying. Int J Adv Manufact Tech. 2016;86:2937–43. doi: 10.1007/s00170-016-8407-9.
[33] Chérif A, Rekik H, Escoda L, Khitouni M, Doghri F, Saurina J, et al. Structural and thermal characterizations of the solid-state reaction between Ni, Al, and Ti powders during mechanical alloying. J Therm Anal Calorimetry. 2016;125:721–7. doi: 10.1007/s10973-016-5355-4.
[34] Smirnov V, Shalunov E, Yanyushkin A, Danilov P. Formation of the structure and properties of composite materials based on copper powder during its reactionary mechanical alloying with titanium, carbon and oxygen. MATEC Web Confer. 2021;344:01017. doi: 10.1051/matecconf/202134401017.
[35] Ghadimi M, Shokuhfar A, Zolriasatein A, Rostami HR. Morphological and structural evaluation of nanocrystalline NiTiCu shape memory alloy prepared via mechanical alloying and annealing. Materials Letters. 2013;90:30–3. doi: 10.1016/j.matlet.2012.09.008.
[36] Zhu J, Wu HH, Wu Y, Wang H, Zhang T, Xiao H, et al. Influence of Ni4Ti3 precipitation on martensitic transformations in NiTi shape memory alloy: R phase transformation. Acta Mater. 2021;207:116665. doi: 10.1016/j.actamat.2021.116665.
[37] Ryu H, Lee ZF, Kim JY, Choi S, Sim GD. Cyclic stability in NiTi and NiTiCu thin films: Role of precipitates in low- and high-cycle regimes. Scr Mater. 2024;250:116189. doi: 10.1016/j.scriptamat.2024.116189.
[38] Yuuu H, Qiu Y, Young ML. Influence of Ni4Ti3 precipitate on pseudoelasticity of austenitic NiTi shape memory alloys deformed at high strain rate. Mater Sci Eng A. 2021;804:140753. doi: 10.1016/j.msea.2021.140753.